2-21-2009

Low Temperature, Organic-Free Synthesis of $Ba_3B_6O_9(OH)_6$ Nanorods and ß-BaB_2O_4 Nanospindles

Rui Li

Xinyoung Tao

Xiaodong Li
University of South Carolina - Columbia, lixiao@cec.sc.edu

Publication Info

Published in *Journal of Materials Chemistry*, Volume 19, Issue 7, 2009, pages 983-987.

This article was first published by the Royal Society of Chemistry and can be found at http://dx.doi.org/10.1039/B816518A
• Li, R., Tao, X., & Li, X. (21 February 2009). Low Temperature, Organic-Free Synthesis of $Ba_3B_6O_9(OH)_6$ Nanorods and ß-BaB_2O_4 Nanospindles. Journal of Materials Chemistry, 19(7), 983 – 987. http://dx.doi.org/10.1039/B816518A

Low temperature, organic-free synthesis of $Ba_3B_6O_9(OH)_6$ nanorods and β-BaB_2O_4 nanospindles†

Rui Li, Xinyong Tao and Xiaodong Li*

Received 22nd September 2008, Accepted 12th November 2008
First published as an Advance Article on the web 19th December 2008
DOI: 10.1039/b816518a

Using a low temperature, organic-free hydrothermal technique, single-crystalline barium polyborate $Ba_3B_6O_9(OH)_6$ (BBOH) nanorods were synthesized. It was found that β-BaB_2O_4 (BBO) nanospindles can be achieved by annealing the BBOH nanorods at a relatively low temperature of 810 °C. Transmission electron microscopy (TEM), X-ray diffraction (XRD), and X-ray photoelectron spectroscopy (XPS) techniques were used to characterize these nanomaterials. The formation mechanisms are discussed in conjunction with the crystallographic characteristics and surface energy of the BBOH nanorods and BBO nanospindles. UV-vis absorption spectra demonstrated that both BBOH nanorods and BBO nanospindles are transparent from the ultraviolet to the visible regions.

Introduction

One dimensional (1D) metal borate nanomaterials have attracted tremendous attention due to their good chemical inertness, high-temperature stability, excellent mechanical properties, and low thermal expansion coefficient.[1–9] Barium borate has potential applications in radiation shielding,[10] lubricating additives[11] and dielectric devices.[12] It has two crystalline phases with a transition temperature of 925 °C, namely, the high temperature phase α-barium borate and the low temperature phase β-barium borate, β-BaB_2O_4 (BBO). BBO is a well-known nonlinear optical material with a high second-order nonlinear susceptibility (d_{eff} = 2.2 pm/V), wide transparency range (189 nm–3500 nm), and high damage threshold.[13–15] BBO bulk crystals are generally grown by high temperature methods, such as the modified Kyropoulos and Czochralski techniques.[16–18] To date, only a couple of methods have been used to synthesize barium borate nanomaterials. BBO nanoparticles were synthesized *via* coprecipitation using different bases as precipitants by Zhou *et al.*[19] Network-like BBO nanostructures were produced by a sol-gel method.[20] BBO nanofilms were prepared by sol-gel deposition[21] and metal organic chemical vapor deposition.[22] To date only one paper reported the successful production of bulk barium polyborate, $Ba_3B_6O_9(OH)_6$ (BBOH), which is the first reported chain borate in which the boron atoms are all tetrahedrally coordinated by oxygen atoms.[23] BBOH nanomaterials, however, have not been reported in the literature.

In this paper, we report the low temperature, organic-free hydrothermal synthesis of single crystalline BBOH nanorods. Moreover, we found that single crystalline BBO nanospindles can be easily obtained by annealing the BBOH nanorods at a relatively low temperature of 810 °C. Both BBOH and BBO were transparent from the ultraviolet to the visible regions.

Department of Mechanical Engineering, University of South Carolina, 300 Main Street, Columbia, South Carolina, 29208, USA. E-mail: lixiao@engr.sc.edu; Fax: (+1) 803-777-0106; Tel: (+1) 803-777-8011

† This paper is part of a *Journal of Materials Chemistry* theme issue on Nanotubes and Nanowires. Guest editor: Z. L. Wang.

Experimental

All chemicals used in our experiments were purchased and used without further purification. Barium chloride dihydrate ($BaCl_2 \cdot 2H_2O$) was purchased from Alfa. Boric acid (H_3BO_3) and sodium hydroxide (NaOH) were purchased from Fisher.

In a typical experiment, 2 mmol of $BaCl_2 \cdot 2H_2O$, 3 mmol of H_3BO_3, and 4 mmol of NaOH were dissolved in 12 ml distilled water under constant magnetic stirring at room temperature. Then, the above suspension was transferred into a 23 ml Teflon-lined stainless steel autoclave. The autoclave was maintained at a fixed temperature of 160 °C for 8 h without stirring or shaking, and then was allowed to cool to room temperature naturally. The precipitate was separated by centrifugation, washed with distilled water and absolute ethanol three times, respectively, and then dried at room temperature. The as-prepared powders were placed in an alumina boat and annealed at 810 °C for 3 h in air.

The products were first analyzed by X-ray diffraction (XRD, Rigaku DMax 2200 using Cu Kα radiation). A few drops of ethanol solution containing the as-prepared products were deposited onto copper grids for transmission electron microscopy (TEM, Hitachi H-8000) and high-resolution transmission electron microscopy (HRTEM, JEOL JEM 2010F) studies. The solvent was then vaporized under ambient conditions. Ultraviolet-visible (UV-vis) absorbance studies were performed using a Beckman Coulter 640 DU spectrophotometer and quartz cuvettes from Starna. Elemental compositions and oxidation states were determined by X-ray photoelectron spectroscopy (XPS), a Kratos Axis Ultra DLD instrument equipped with a monochromated Al Kα X-ray source and hemispherical analyzer capable of an energy resolution of 0.5 eV. Thermogravimetric analysis (TGA) and differential thermal analysis (DTA) were performed using a Thermal Analysis Instruments SDT2960 Thermogravimetric Analyzer, and the sample was scanned at a rate of 20 °C per minute. Fourier transform infrared (FTIR) analysis was performed using a Perkin Elmer Spectrum 100 FTIR spectrometer fitted with a Diamond ATR attachment.

Results and discussion

Fig. 1a shows a representative XRD pattern of the sample synthesized *via* the hydrothermal method at 160 °C for 8 h. All the peaks can be readily indexed to the monoclinic phase of BBOH (JCPDS file, no. 01-071-2501), with lattice constants of $a = 6.99$, $b = 7.14$ and $c = 11.92$ Å, and space group of $P2/c$. No impurity peaks were observed. The low and high magnification TEM images (Fig. 1b and c) show that the synthesized BBOH exhibits rod-like morphology with an average diameter of 115 nm and lengths ranging from 1 to 3 μm. The representative HRTEM image (Fig. 1d) and selected area electron diffraction (SAED) pattern (Fig. 1e) indicate that the synthesized BBOH nanorods are single crystals with the growth orientation along the [102] direction. No defects such as dislocations and twins were found. The measured distance between the lattice fringes for the (102) planes is 0.45 nm.

For the BBOH nanorods, the weight loss was found to be about 7.6% in the range of 100–600 °C when heated in air (Fig. 2), in good agreement with the weight loss from the removal of the adsorbed water molecules and the hydroxyl groups. Analysis of the TGA curve (Fig. 2) reveals that the weight loss occurred in two stages, as in the case for some reported borate hydrates.[24] The first stage is in the temperature range of 125–240 °C with a weight loss of 2.6% and the second stage proceeds in the range of 300–600 °C with a weight loss of 5.0%. These two weight loss stages agree well with the two endothermic effects at about 197 °C and 382 °C in the DTA curve (Fig. 2), which are 57 °C and 32 °C higher than those of bulk BBOH, respectively.[23] The exothermic effect at about 763 °C can be attributed to the crystallization of the BBO crystals, which will be discussed in the following paragraphs.

Fig. 3a shows the XRD pattern of the product obtained after annealing the BBOH nanorods at 810 °C for 3 h in air. All the

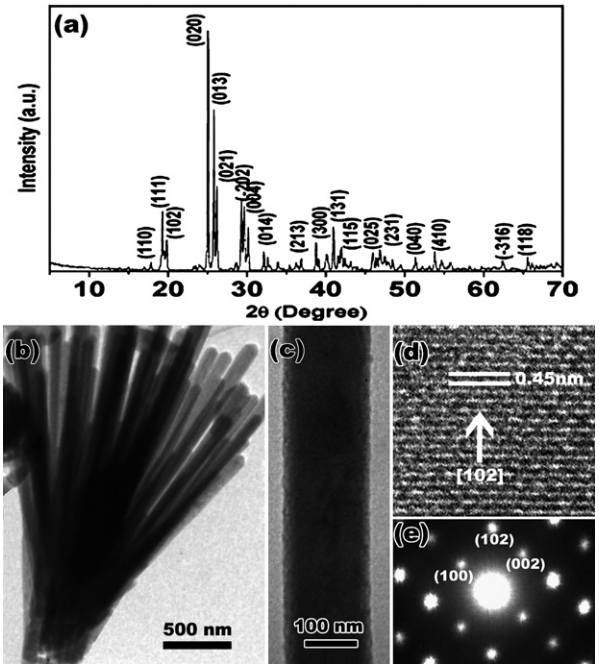

Fig. 1 (a) XRD pattern of the sample synthesized *via* the hydrothermal method at 160 °C for 8 h, (b) low magnification TEM image, (c) high magnification TEM image, (d) HRTEM image, and (e) corresponding SAED pattern of BBOH nanorods.

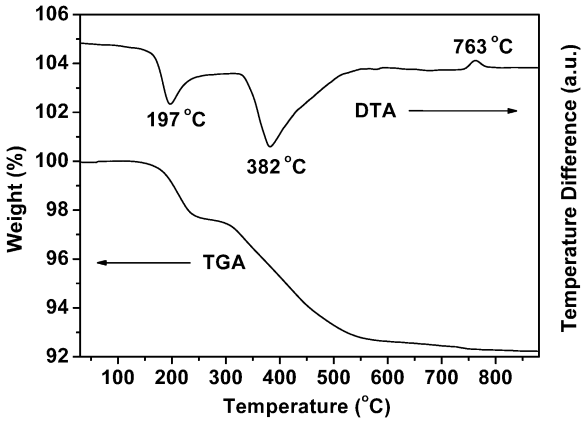

Fig. 2 TGA and DTA curves of BBOH nanorods.

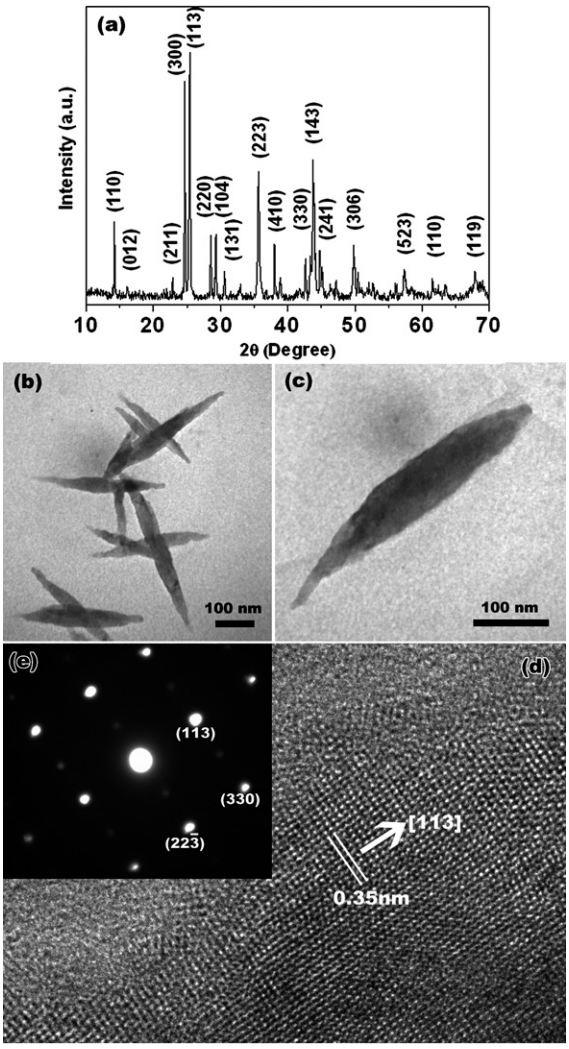

Fig. 3 (a) XRD pattern, (b) low magnification TEM image, (c) high magnification TEM image, (d) HRTEM image, and (e) corresponding SAED pattern of BBO nanospindles.

peaks can be readily indexed to the hexagonal phase of BBO (JCPDS file, no. 80-1489), with lattice constants of $a = 12.53$, $c = 12.73$ Å and space group of *R3c*. The TEM images (Fig. 3b and c) reveal that the obtained BBO exhibits spindle-like morphology with an average length of 600 nm and widths ranging from 35 to 60 nm in the widest section. The HRTEM image and SAED pattern (Fig. 3d and e) further reveal that the BBO nanospindles are single crystals with the growth orientation of the [113] direction. No defects such as dislocations and twins were found. The measured distance between the lattice fringes for the (113) planes is 0.35 nm.

XPS analysis was carried out to further characterize the BBOH nanorods and BBO nanospindles (Fig. 4). The binding energies were corrected by taking the C 1s core level at 284.8 eV for the two samples. Both survey spectra, as shown in Fig. 4a, exhibit Ba 3p, Ba 3d, Ba 4d, Ba 4p, B 1s, O 1s and C 1s core levels, and Ba MNN Auger peak. In Fig. 4b, the peaks at 779.8 eV and 795.1 eV in the BBOH curve and the peaks at 780.1 eV and 795.4 eV in the BBO curve can be attributed to Ba $3d_{5/2}$ and Ba $3d_{3/2}$, respectively. B 1s and Ba $4p_{1/2}$ peaks overlapped in the survey spectra, and XPSPEAK software (Version 4.1) was used to fit this overlapped peak with two components, *i.e.*, B 1s and Ba $4p_{1/2}$ peaks. In Fig. 4c, the peak at 191.7 eV in the BBOH curve and the peak at 191.9 eV in the BBO curve correspond to the B 1s core level. The binding energies of Ba 3d and B 1s of BBO are 0.3 eV and 0.2 eV greater than those of BBOH, respectively, due to the different chemical structures of these two materials. In Fig. 4d, the O 1s peaks at 531.27 eV in the BBOH curve and at 531.8 eV in the BBO curve suggest that the oxygen exists as O^{2-} species in the BBOH nanorods and BBO nanospindles. These results for BBO nanospindles are in good agreement with the values for crystalline BBO reported in the literature.[20,25]

Fig. 5 shows the UV-vis absorption spectra of BBOH nanorods and BBO nanospindles. It can be seen that both BBOH and BBO are transparent up to 210 nm (5.90 eV) within the limitation of the instrument whose working range is 210–790 nm. The absorption spectra are relatively featureless, and the broad and overall constant low absorbance from 210 to 790 nm is consistent with the reported values for bulk BBO single crystals[26] and

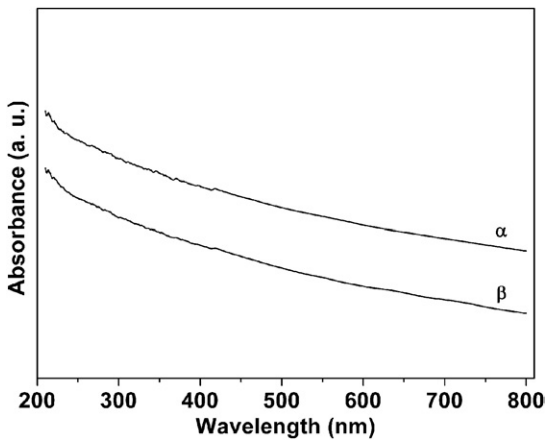

Fig. 5 UV-vis absorption spectra of (α) BBOH nanorods and (β) BBO nanospindles.

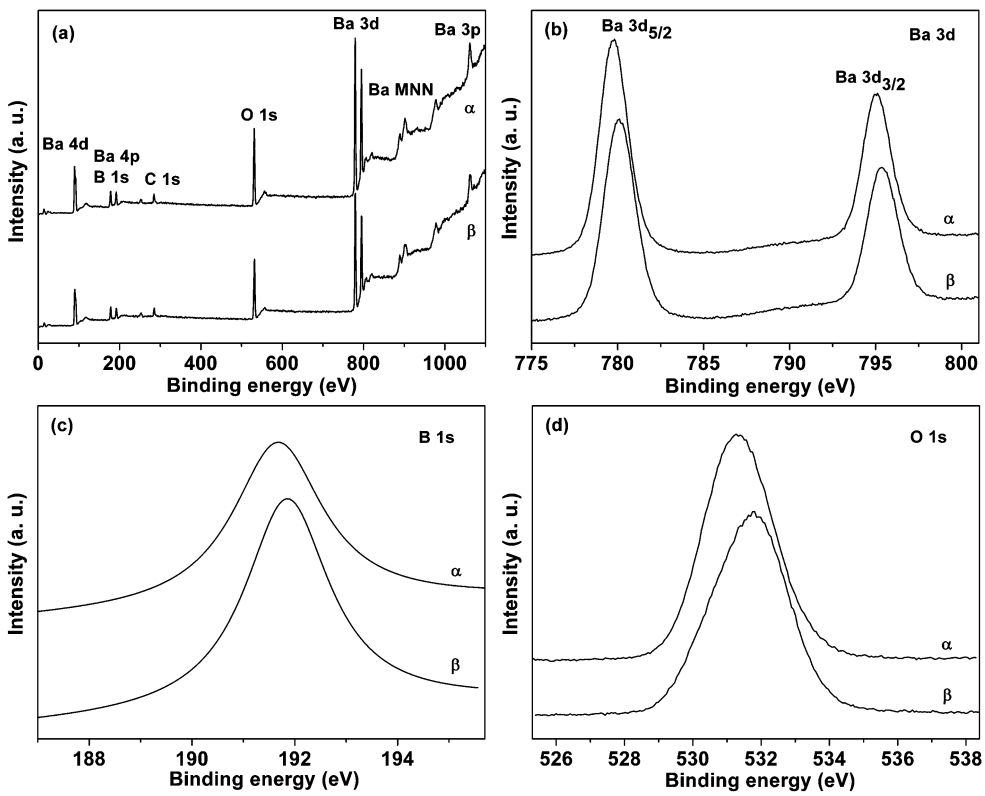

Fig. 4 XPS spectra of (α) BBOH nanorods and (β) BBO nanospindles. (a) Survey spectra, (b), (c), and (d), detailed spectra of Ba 3d, B 1s and O 1s core levels, respectively.

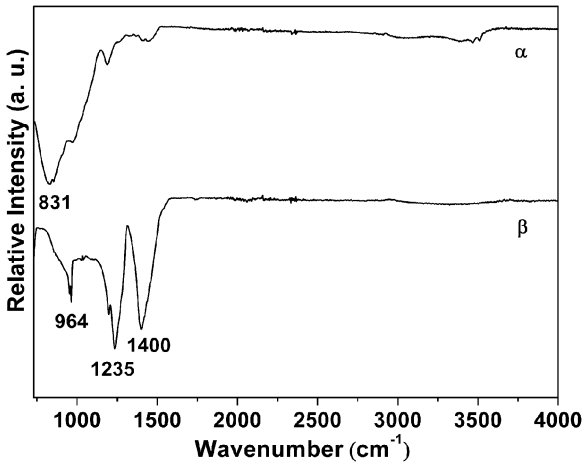

Fig. 6 FTIR spectra of (α) BBOH nanorods and (β) BBO nanospindles.

network-like nanomaterials,[20] thus demonstrating that it is transparent from the ultraviolet to the visible regions.

Fig. 6 shows the FTIR spectra of the BBOH nanorods and BBO nanospindles. The BBOH nanorods show an absorption in the range of 4000–2700 cm^{-1}, indicating the presence of hydroxyl groups. The broad strong bands observed close to 831 cm^{-1} are due to the vibrations of tetrahedral $(BO_4)^{5-}$ groups, that are the basic units of the BBOH structure.[23] The FTIR spectrum of the BBO nanospindles exhibits broad absorptions in the 900–1500 cm^{-1} range. The absorption peak at 1235 cm^{-1} results from the B–O stretching in the $(BO_3)^{3-}$ unit, which is a component of the $(B_3O_6)^{3-}$ ring. The peaks observed at 964 and 1400 cm^{-1} are attributed to B–O extra-ring stretching.[27] The detailed FTIR analyses suggest that the BBO nanospindles have the characteristics of bulk BBO crystals.

Based on the above experimental results, the formation mechanisms of the BBOH nanorods and BBO nanospindles are proposed. The whole process, which is described in the following reactions,

$$3\ Ba^{2+} + 6\ H_3BO_3 + 6\ OH^- = Ba_3B_6O_9(OH)_6\downarrow + 9\ H_2O$$

$$Ba_3B_6O_9(OH)_6 = 3\ BaB_2O_4 + 3\ H_2O\uparrow$$

can be schematically illustrated in Fig. 7. Flocculant precipitates, as we observed in the experiments, were formed immediately after dissolving the reactants in the aqueous solution under intensive stirring. This suspension was transferred into a 23 ml Teflon-lined stainless steel autoclave. The autoclave was maintained at a fixed temperature of 160 °C for 8 h without stirring or shaking. First, as shown in Fig. 7a, nuclei were formed from the flocculant precipitates in the suspension under hydrothermal conditions.[28,29] Second, the nuclei grew by consuming the ambient raw materials (Fig. 7b). Third, the larger nanoparticles fell to the bottom of the autoclave and began to aggregate most probably by electrostatic gravitation and intermolecular force (Fig. 7c). The smaller ones were attached to the aggregate and extended in a certain way because the anisotropic growth of the nanocrystals in a template-free method is generally related to the different surface energies of different crystal planes of the nanocrystals. Those planes with high surface energy have a strong tendency to capture smaller nanoparticles from the reaction solution in order to reduce their surface energy.[28,29] This leads to growth along those planes and formation of the 1D BBOH nanorod bundles in Fig. 7d. After ultrasonic treatment BBOH nanorods were obtained.

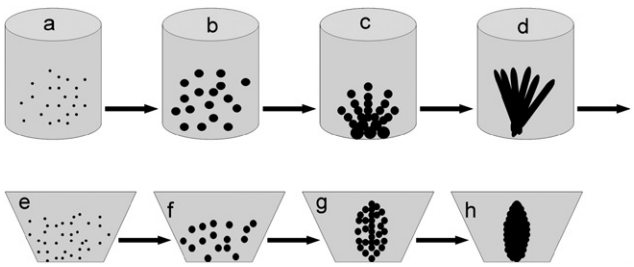

Fig. 7 Schematic diagram showing the growth processes of BBOH nanorods in the autoclave (a–d) and BBO nanospindles in the alumina boat (e–h).

To prepare the BBO nanomaterials, the as-prepared BBOH nanorods were annealed at 810 °C for 3 h in air. The BBOH nanorods contain water in the form of both hydroxyl ions and adsorbed water molecules. This allows one to rationalize a complex process of dehydration of borates at elevated temperatures which involves elimination of individual adsorbed water molecules and hydroxyl groups, due to association of boron-containing anions (see TGA and DTA curves in Fig. 2). Dehydration of borates is accompanied by a specific effect of borate rearrangement,[30] namely, dehydration causes complete destruction of the crystal lattice and transition of the BBOH nanorods into the amorphous state; further heating leads to crystallization including the nucleation and growth processes as solid-state reaction. First, in Fig. 7e, nuclei were formed from the amorphous solid under heat-treatment conditions. Second, the nuclei grew by consuming the ambient amorphous solid (Fig. 7f). Third, in Fig. 7g, the nanoparticles aggregated in a certain way driven likely by electrostatic attractions and intermolecular forces. Finally single crystal BBO nanospindles were formed (Fig. 7h).

Spindle-shaped nanostructures have great potential applications in the field of optics;[31–33] the detailed optical and optoelectronic properties will be studied further in the future.

Conclusions

Barium polyborate BBOH nanorods were synthesized *via* a low temperature, organic-free hydrothermal route. These nanorods can be easily transformed into BBO nanospindles through heat treatment at 810 °C for 3 h. Both BBOH nanorods and BBO nanospindles are transparent from the ultraviolet to the visible regions.

Acknowledgements

Financial support for this study was provided by the National Science Foundation (CMMI-0653651 and EPS-0296165), the ACS Petroleum Research Fund (ACS PRF 40450-AC10), and the University of South Carolina NanoCenter. We thank Douglas Blom and Soumitra Ghoshroy (the University of South Carolina EM Center) for TEM technical support.

References

1 R. Z. Ma, Y. Bando and T. Sato, *Appl. Phys. Lett.*, 2002, **81**, 3467.
2 X. Y. Tao, X. N. Wang and X. D. Li, *Nano Lett.*, 2007, **7**, 3173.
3 X. Y. Tao and X. D. Li, *Nano Lett.*, 2008, **8**, 505.
4 Y. Li, Z. Y. Fan, J. G. Lu and R. P. H. Chang, *Chem. Mater.*, 2004, **16**, 2512.
5 Y. C. Zhu, Y. Bando and R. Z. Ma, *Adv. Mater.*, 2003, **15**, 1377.
6 C. C. Tang, E. M. Elssfah, J. Zhang and D. F. Chen, *Nanotechnology*, 2006, **17**, 2362.
7 J. Zhang, Y. Huang, J. Lin, X. X. Ding, Z. X. Huang, S. R. Qi and C. C. Tang, *J. Phys. Chem. B*, 2005, **109**, 13060.
8 H. S. Song, E. M. Elssfah, J. Zhang, J. Lin, J. J. Luo, S. J. Liu, Y. Huang, X. X. Ding, J. M. Gao, S. R. Qi and C. C. Tang, *J. Phys. Chem. B*, 2006, **110**, 5966.
9 R. Z. Ma, Y. Bando, T. Sato, C. C. Tang and F. F. Xu, *J. Am. Chem. Soc.*, 2002, **124**, 10668.
10 S. Singh, A. Kumar, D. Singh, K. S. Thind and G. S. Mudahar, *Nucl. Instr. and Meth. in Phys. Res. B*, 2008, **266**, 140.
11 N. Liu, Y. M. Tian, L. X. Yu, Q. J. Li, F. Y. Meng, Y. H. Zheng, G. Y. Zhang, Z. H. Liu, J. Li and F. M. Jiang, *J. Alloy. Compd.*, 2008, **466**, L11.
12 C. R. Raja, R. Gobinathan and F. D. Gnanam, *Cryst. Res. and Technol.*, 1993, **28**, 737.
13 D. Eimerl, L. Davis, S. Velsko, E. K. Graham and A. Zalkin, *J. Appl. Phys.*, 1987, **62**, 1968.
14 D. N. Nikogosyan, *Appl. Phys. A*, 1991, **52**, 359.
15 Y. N. Xia, P. D. Yang, Y. G. Sun, Y. Y. Wu, B. Mayers, B. Gates, Y. D. Yin, F. Kim and H. Q. Yan, *Adv. Mater.*, 2003, **15**, 353.
16 H. Kouta, Y. Kuwano, K. Ito and F. Marumo, *J. Cryst. Growth*, 1991, **114**, 676.
17 L. K. Cheng, W. Bosenberg and C. L. Tang, *Prog. Cryst. Growth Charact.*, 1990, **20**, 9.
18 R. S. Feigelson, R. J. Raymakers and R. K. Route, *Prog. Cryst. Growth Charact.*, 1990, **20**, 115.
19 Y. F. Zhou, M. C. Hong, Y. Q. Xu, B. Q. Chen, C. Z. Chen and Y. S. Wang, *J. Cryst. Growth*, 2005, **276**, 478.
20 Q. R. Zhao, X. Zhu, X. Bai, H. H. Fan and Y. Xie, *Eur. J. Inorg. Chem.*, 2007, 1829.
21 C. Lu, S. S. Dimov and R. H. Lipson, *Chem. Mater.*, 2007, **19**, 5018.
22 S. Wersand-Quell, G. Orsal, P. Thevenin and A. Bath, *Thin Solid Films*, 2007, **515**, 6507.
23 Z. T. Yu, Z. Shi, W. Chen, Y. S. Jiang, H. M. Yuan and J. S. Chen, *J. Chem. Soc., Dalton Trans.*, 2002, 2031.
24 Y. E. Anderson, S. K. Filatov, I. G. Polyakova and R. S. Bubnova, *Glass Phys. Chem.*, 2004, **30**, 450.
25 V. V. Atuchin, V. G. Kesler, A. E. Kokh and L. D. Pokrovsky, *Appl. Surf. Sci.*, 2004, **223**, 352.
26 T. Yogo, K. Kikuta, K. Niwa, M. Ichida, A. Nakamura and S. Hirano, *J. Sol-Gel Sci. Technol.*, 1997, **9**, 201.
27 U. Moryc and W. S. Ptak, *J. Mol. Struct.*, 1999, **511–512**, 241.
28 B. Liu and H. C. Zeng, *J. Am. Chem. Soc.*, 2003, **125**, 4430.
29 M. F. Ye, H. Z. Zhong, W. J. Zheng, R. Li and Y. F. Li, *Langmuir*, 2007, **23**, 9064.
30 P. P. Fedorov, A. E. Kokh and N. G. Kononova, *Russ. Chem. Rev.*, 2002, **71**, 651.
31 J. Geng, J. J. Zhu, D. J. Lu and H. Y. Chen, *Inorg. Chem.*, 2006, **45**, 8403.
32 M. F. Zhang, H. Fan, B. J. Xi, X. Y. Wang, C. Dong and Y. T. Qian, *J. Phys. Chem. C*, 2007, **111**, 6652.
33 H. Wang, D. W. Brandl, F. Le, P. Nordlander and N. J. Halas, *Nano Lett.*, 2006, **6**, 827.